

Plasmon-Sampled Surface-Enhanced Raman Excitation Spectroscopy[†]

Christy L. Haynes and Richard P. Van Duyne*

Department of Chemistry, Northwestern University, Evanston, Illinois 60208-3113

Received: December 17, 2002; In Final Form: February 13, 2003

This work presents the first systematic study of the surface-enhanced Raman-scattering (SERS) properties of nanosphere lithography (NSL) derived Ag nanoparticles. Furthermore, it demonstrates the necessity of correlating nanoparticle structure and localized surface plasmon resonance (LSPR) spectroscopic data in order to effectively implement SERS on nanofabricated surfaces that have narrow (~ 100 nm) LSPR line widths. Using nanoparticle substrates that are structurally well characterized by atomic force microscopy, the relationship between the LSPR extinction maximum (λ_{max}) and the SERS enhancement factor (EF) is explored in detail using the innovative approach of plasmon-sampled surface-enhanced Raman excitation spectroscopy (PS-SERES). PS-SERES studies were performed as a function of excitation wavelength, molecular adsorbate, vibrational band, and molecule-localized resonance or nonresonance excitation. In each case, high S/N ratio spectra are achieved for samples with an LSPR λ_{max} within a ~ 120 -nm window that encompasses both the excitation wavelength and the scattered wavelength. These results unambiguously demonstrate a systematic approach to the optimization of SER spectra on nanoparticle substrates with large interparticle spacings and consequently, weak or no electromagnetic coupling. In fact, this work demonstrates the largest SERS, $\text{EF} > 1 \times 10^8$, and SERRS, $\text{EF} > 7 \times 10^9$, enhancement factors measured to date on nanostructured substrates. The observation that $\text{EF}_{\text{SERRS}}/\text{EF}_{\text{SERS}} \sim 40$ and $E_{\text{RRS}}/E_{\text{Pre-RRS}} \sim 40$ in the $\text{Fe}(\text{bpy})_3^{2+}$ system illustrates that this adsorbate, with its molecule-localized electronic transition, does not damp the nanoparticle-localized LSPR and that the SERS and RRS effects are strictly multiplicative.

Introduction

The current widespread interest in size-dependent optical properties of nanomaterials¹ is a consequence of their many applications in research areas such as chemosensors,² biosensors,³ nanoparticle optics,⁴ and surface-enhanced spectroscopy.^{5,6} Recently, interest in surface-enhanced Raman spectroscopy (SERS) has been rekindled by the observation of single-molecule SERS.^{7,8} Single-molecule SER spectra are characterized by enormous EFs ($\sim 10^{14}$ – 10^{16}) and temporal fluctuation in the vibrational spectrum. The mechanism is not understood, though many research groups are actively pursuing this topic. It is not yet clear if single-molecule SERS occurs at a single nanoparticle or if a nanoparticle assembly (viz., dimer, aggregate, etc.) is required. The work presented here focuses not on the single-molecule SERS phenomenon, but normal SERS. In fact, this work reports the first SERS data measured from nanosphere lithography (NSL) samples.

Surprisingly, in the 25 years since the discovery of the SERS effect,⁹ there has never been a detailed comparison of the localized surface plasmon resonance (LSPR) spectra of highly ordered, structurally well-defined, nanoparticle surfaces and the surface-enhanced Raman excitation spectra (SERES) even though they are intimately linked through the electromagnetic (EM) enhancement mechanism.⁵ There are more than 4000 papers concerning SERS and its many applications; however, less than 30 of these address SERES. The paucity of SERES data in the literature is a consequence of the difficulty of SERES experiments, its typically low data point density, and therefore, its low information content.

The traditional wavelength-scanned approach to SERES (WS-SERES)^{10–12} involves the measurement of SER spectra from a single substrate with many laser excitation wavelengths λ_{ex} . WS-SERE spectra are plots of Raman intensity for a particular vibrational band, λ_{vib} , versus λ_{ex} . These plots report the optimized λ_{ex} for that specific substrate, adsorbate, and local dielectric environment. The inherent difficulty in WS-SERES lies in the fact that the number of data points is limited either by excitation and/or detection tunability. WS-SERES studies with low data point density have reported $\text{EF} = 5 \times 10^6$ and 2×10^6 for microlithographically fabricated Ag nanoparticle arrays^{10,13} and Ag island films,¹⁴ respectively. Broadly tunable WS-SERES experiments are now technically possible using CW mode-locked Ti:Sapphire lasers, their harmonics, and optical parametric amplifiers in combination with a triple spectrograph/CCD detector; however, such equipment is not widely available. Consequently, to our knowledge, only one such WS-SERES experiment has ever been reported.¹¹

In contrast, the innovative approach to SERES detailed herein describes a method, plasmon-sampled-SERES (PS-SERES), that yields information rich SERE spectra using readily available instrumentation. The PS-SERE spectra reported here have been measured under ambient conditions using irreversibly bound adsorbates and nanoparticle surfaces fabricated by nanosphere lithography.¹ Previous work has demonstrated that these nanoparticle surfaces have LSPRs that are extremely sensitive to their size and shape and are spectrally narrow (viz., < 100 nm).⁴ In the PS-SERES experiment, the LSPR and SERS measurements are both spatially resolved and spatially correlated using far-field optical microscopy. By interchanging a white light source with UV–vis extinction detection and a laser light source with Raman detection, it is possible to measure the LSPR (~ 25 –

[†] Part of the special issue "Arnim Henglein Festschrift".

* To whom correspondence should be addressed. E-mail: vanduyne@chem.northwestern.edu.

μm -diameter spot size) and SER ($\sim 4\text{-}\mu\text{m}$ -diameter spot size) spectra from the same domain on each sample. Thus, PS-SERE spectra plot the SERS intensity or EF for a particular adsorbate vibrational mode versus the LSPR λ_{max} . Empirically, the SERS signal intensity does not vary from spot to spot on the $25\text{-}\mu\text{m}$ scale. The results garnered using the PS-SERES technique are information rich when compared to results gained using the WS-SERES technique. Instead of determining the best λ_{ex} to use with a particular substrate, adsorbate, and environment, the PS-SERES gives generalized optimization conditions. Accordingly, the results of this work increase the practical utility of the SERS method.

An entire PS-SERES experiment (viz., ~ 100 data points) is done with a single λ_{ex} . Consequently, readily available fixed wavelength lasers and notch filter/single-monochromator/CCD detection systems may be used. The number of data points obtainable in PS-SERES is limited only by the number of sample regions with different LSPR λ_{max} characteristics and the number of samples measured. In this work, we exploit the naturally occurring variation in the LSPR λ_{max} on each sample caused by (1) the small, random structural variations inherent in the NSL fabrication technique;¹⁵ (2) inhomogeneities in the local dielectric environment due to adsorbed water;^{16–18} and (3) any residual electromagnetic coupling effects.¹⁹ Previous work has firmly established the sensitivity of the LSPR λ_{max} of NSL-fabricated nanoparticles to all the details of their local dielectric environment.^{2,3,20} An adsorbed water layer is impossible to eliminate under ambient conditions due to the high number density of oxide groups at the surface of the glass substrate.²¹ Because PS-SERES benefits from the distribution of LSPR λ_{max} values, all extinction and SER spectra presented herein are measured from NSL-fabricated Ag nanoparticles on glass substrates where the standard deviation of a Gaussian fit to the LSPR λ_{max} distribution is ~ 10 nm.

Experimental Section

Materials. Ag (99.99%, 0.04 in. diameter) was purchased from D. F. Goldsmith (Evanston, IL). Glass substrates were 18-mm-diameter, No. 2 coverslips from Fisher Scientific (Fairlawn, VA) and ruby-red muscovite mica from Asheville-Schoonmaker (Newport News, VA) cut to an 18-mm diameter with a hole punch. Pretreatment of glass substrates required H_2SO_4 , H_2O_2 , and NH_4OH , all purchased from Fisher Scientific (Fairlawn, VA). Surfactant-free, white, carboxyl-substituted polystyrene latex nanospheres with diameters (D) of 280 ± 4 , 310 ± 8 , and 400 ± 8 nm were obtained from Interfacial Dynamics Corporation (Portland, OR). Tungsten vapor deposition boats were purchased from R. D. Mathis (Long Beach, CA). Benzenethiol, 1,4-benzenedithiol, and 3,4-dichlorobenzenethiol were purchased from Aldrich (Milwaukee, WI) and used as received. $\text{Fe}(\text{bpy})_3(\text{PF}_6)_2$ was synthesized as previously reported.²² Precursors for $\text{Fe}(\text{bpy})_3(\text{PF}_6)_2\text{--Fe}(\text{NH}_4)_2(\text{SO}_4)_2\cdot 6\text{H}_2\text{O}$ (99.997%), 2,2'-bipyridine (99%), and NH_4PF_6 (99.99%)—were all purchased from Aldrich (Milwaukee, WI) and used as received. Methanol was purchased from Fisher Scientific (Fairlawn, VA) and ethanol was purchased from Pharmco (Brookfield, CT). For all steps of substrate preparation, ultrapure water ($18.2 \text{ M}\Omega \text{ cm}^{-1}$) from a Millipore academic system (Marlborough, MA) was used. Nitrogen used for drying was purchased from Air Products (Allentown, PA) and passed through a particulate filter and a tube packed with Drierite (W. A. Hammond Drierite Co., Xenia, OH) before use.

Nanosphere Lithography. Borosilicate glass substrates were pretreated in two steps (1) piranha etch, 3:1 H_2SO_4 :30% H_2O_2

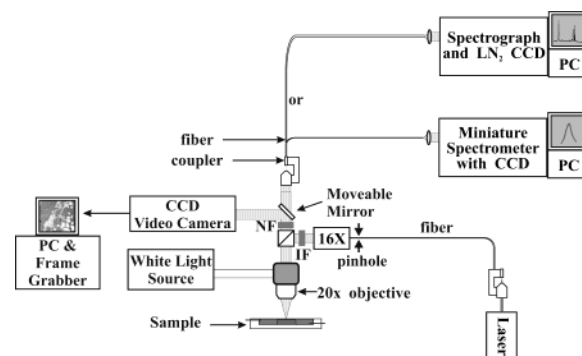


Figure 1. Schematic diagram of the PS-SERES apparatus.

at $80\text{ }^\circ\text{C}$ for 1 h, was used to clean the substrate, and (2) base treatment, 5:1:1 $\text{H}_2\text{O}:\text{NH}_4\text{OH}:30\% \text{H}_2\text{O}_2$ with sonication for 1 h, was used to render the surface hydrophilic. Approximately $2\ \mu\text{L}$ of undiluted nanosphere solution (10% solids) were drop coated onto each substrate and allowed to dry in ambient conditions. The metal films were deposited in a modified Consolidated Vacuum Corporation vapor deposition system²³ with a base pressure of 10^{-7} Torr. The mass thickness (d_m) and deposition rate for each film were measured using a Leybold Inficon XTM/2 quartz-crystal microbalance (QCM) (East Syracuse, NY). After metal deposition, removal of the polystyrene nanospheres was achieved by sonication in absolute ethanol for 3 min.

Atomic Force Microscopy. Atomic force microscopy (AFM) was used to explore structural variation and verify that NSL-fabricated samples met expected topographic characteristics. All images (not shown) were collected under ambient conditions with a Digital Instruments Nanoscope III AFM. The etched Si nanoprobe tips (Digital Instruments, Santa Barbara, CA) used to acquire the images have resonant frequencies between 285 and 315 kHz. These tips are conical in shape with a cone angle of 20° and have an effective radius of curvature of 10 nm. Data were collected in the intermittent contact mode using a scan rate of 2.5 Hz. The scan head had a range of $13\ \mu\text{m} \times 13\ \mu\text{m}$.

PS-SERES Apparatus. The general concept of the PS-SERES experiment is that extinction and SER spectra are captured from the same area on a nanostructured sample. To achieve this goal, it is necessary to interchange a white light source with UV–vis extinction detection and a laser light source with Raman detection (Figure 1). PS-SERE spectra are plots of the SERS EF (vide infra) for a particular λ_{vib} versus the LSPR λ_{max} .

Spatially resolved extinction and SER spectra were measured using a modified Nikon Optiphot (Frier Company, Huntley, IL) confocal microscope with a 20x objective in backscattering geometry. When recording an extinction spectrum, the tungsten–halogen microscope lamp provided white light excitation (the laser was blocked from entering the input fiber optic) and the output fiber optic was coupled to an Ocean Optics (Dunedin, FL) model SD2000 spectrometer. When recording a Raman spectrum, excitation was provided by one of the following lasers: Spectra-Physics (Mountain View, CA) model 2060 Ar^+ laser operating at $\lambda_{\text{ex}} = 514.5$ nm, Spectra-Physics model Millennia Vs laser operating at $\lambda_{\text{ex}} = 532.0$ nm, or a Coherent (Santa Clara, CA) model 590 dye laser operating at $\lambda_{\text{ex}} = 632.8$ nm. In each case, the laser light was coupled into a $200\text{-}\mu\text{m}$ -core-diameter fiber using a Thorlabs (Newton, NJ) fiber launch, and appropriate Edmund Scientific (Barrington, NJ) interference filters and Kaiser (Ann Arbor, MI) holographic notch filters were placed in the beam path. For SER spectra, the output fiber

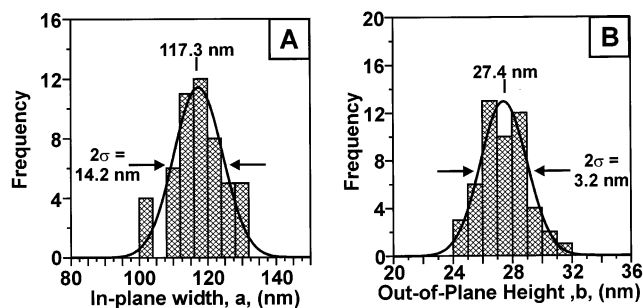


Figure 2. Nanoparticle structural variation on a nanosphere lithography substrate. (A) demonstrates the structural variation, measured using intermittent contact mode AFM, in the in-plane width a for nanoparticles fabricated on a glass substrate using $D = 400$ nm and $d_m = 27$ nm. The absolute values of a are convoluted by the AFM tip radius of curvature. The average measured value of a is 117.3 ± 7.1 nm. (B) demonstrates the topographic variation, measured using intermittent contact mode AFM, in the out-of-plane height b for nanoparticles fabricated on a glass substrate using $D = 400$ nm and $d_m = 27$ nm. The average measured value of b is 27.4 ± 1.6 nm.

optic was coupled to an Acton (Acton, MA) VM-505 monochromator with the entrance slit set at $250 \mu\text{m}$ with a Roper Scientific (Trenton, NJ) Spec-10:400B liquid- N_2 -cooled CCD detector.

Results and Discussion

The results reported herein systematically probe the dependence of the intensity-optimized SERS signal on several important experimental factors. Beyond demonstrating the utility of the PS-SERES technique in optimizing SERS intensity, the goal was to illuminate the stringency of matching conditions between the excitation wavelength, scattering wavelength, and LSPR λ_{max} wavelength. In all reported cases, the data show that the substrate LSPR λ_{max} must fall within a ~ 120 -nm window that includes both the excitation and scattering wavelength. This LSPR λ_{max} window width was empirically determined simply by bounding the window when a sample no longer gave a SERS signal measurable above background. In addition, it is important to note that the reported EFs are calculated using the most conservative values of adsorbate number density possible. In all cases, there is less than a factor of 10 modulation in the measured EF in a given PS-SERE spectrum. The factor of 10 has a large effect on the apparent signal-to-noise ratio because the background signal scales with the SERS signal. The largest window of LSPR λ_{max} values explored in any of the displayed PS-SERES plots is 200 nm; if a NSL sample with a LSPR λ_{max} outside this window is used, no SER spectrum is observed above background.

Origin and Statistical Analysis of the LSPR λ_{max} Distribution. The LSPR λ_{max} for NSL-fabricated Ag nanoparticles on glass substrates varies from domain to domain with a Gaussian distribution having a standard deviation of ~ 10 nm. To better understand the factors that contribute to this distribution, a detailed AFM structural study was performed and the results were compared with the corresponding LSPR data. In this study, 51 randomly chosen individual nanoparticles were examined, each in perfectly packed areas of randomly chosen domains. Parts A and B of Figure 2 show the experimental histograms accompanied with Gaussian fits that describe the variation in the structural parameters on a sample fabricated with $D = 400$ nm and $d_m = 27$ nm Ag on a glass substrate. All parameters derived from the Gaussian fit will be reported as the average value $\pm \sigma$, where σ is the half-width at half-height. The histogram in Figure 2A shows that the average in-plane

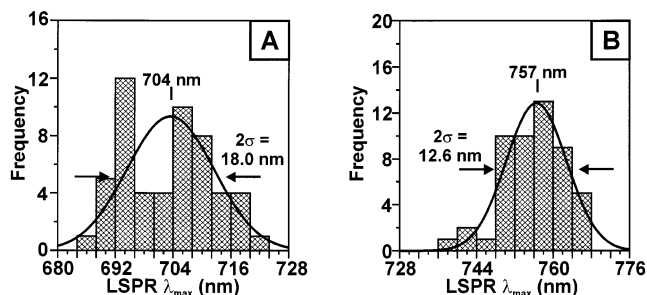


Figure 3. Effect of bulk dielectric environment on LSPR λ_{max} variation for NSL-fabricated Ag nanoparticles. (A) represents LSPR behavior of $D = 390$ nm and $d_m = 25$ nm Ag nanoparticles on glass in the lab ambient environment. The average measured LSPR λ_{max} is 704 ± 9.0 nm. (B) represents LSPR behavior of $D = 400$ nm and $d_m = 40$ nm Ag nanoparticles with an adsorbed monolayer of benzenethiol in a homogeneous ethanol environment. The average measured LSPR λ_{max} is 757 ± 6.3 nm.

nanoparticle width a is 117.3 ± 7.1 nm. Note that the absolute value of the measured in-plane width is artificially increased by ~ 20 nm with respect to the geometric prediction due to convolution by the AFM tip.¹⁵ The histogram in Figure 2B shows that the average out-of-plane nanoparticle height b is 27.4 ± 1.6 nm. These distributions of the nanoparticle structural properties clearly account for some of the LSPR λ_{max} distribution. However, an even more important factor to consider is the effect of inhomogeneities in the local dielectric environment. Parts A and B of Figure 3 compare the LSPR λ_{max} distribution for NSL-fabricated Ag nanoparticles on glass substrates under ambient and adsorbate/solvent environments. The histogram in Figure 3A is constructed from $25\text{-}\mu\text{m}$ -diameter randomly chosen domains on a sample with $D = 390$ nm and $d_m = 25$ nm Ag in ambient laboratory conditions. The average LSPR λ_{max} is 704 ± 9.0 nm. Figure 3B depicts the LSPR λ_{max} variation from a separate sample with $D = 390$ nm and $d_m = 27$ nm Ag after immersion for > 12 h in a 1-mM benzenethiol solution; all measurements were made while the sample was immersed in a homogeneous ethanol environment. Other experiments (not shown) demonstrate that adsorption of benzenethiol decreases the standard deviation of the LSPR λ_{max} distribution by 6% to 8.5 nm. The average LSPR λ_{max} for the benzenethiol-coated substrate in ethanol is 757 nm (an expected red shift due to the higher refractive index of the benzenethiol/ethanol versus air),²⁰ and its standard deviation decreases by 30% to 6.3 nm. Clearly, the inhomogeneous dielectric environment created by adsorbed water plays an important role in the observed LSPR λ_{max} variation.

To quantitatively demonstrate the effect of the water layer on two different substrates, a similar statistical analysis was performed for extinction spectra captured from Ag NSL nanoparticles on both glass and mica substrates in a controlled atmosphere cell. In each case, approximately 50 extinction measurements were performed on isolated, randomly chosen $25\text{-}\mu\text{m}$ -diameter domains both when the NSL samples were initially prepared and after the nanoparticles were exposed to $100\text{-cm}^3/\text{min}$ flow of N_2 for 24 h. These data are presented in Figure 4 as a series of histograms with Gaussian fits. Parts A and B of Figure 4 show the LSPR λ_{max} variation present on glass substrates initially, and after 24 h of N_2 exposure; the average LSPR λ_{max} values are 703 ± 9 and 704 ± 7 nm, respectively. Parts C and D of Figure 4 show the corresponding LSPR λ_{max} variation on mica substrates initially and after 24 h of N_2 exposure; the average LSPR λ_{max} values are 699 ± 5 and 698 ± 4 nm, respectively. These results clearly demonstrate

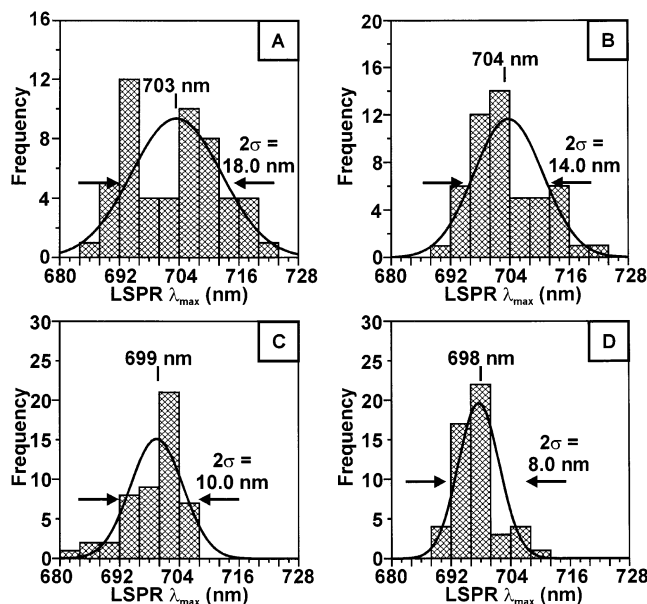


Figure 4. Effect of substrate on LSPR λ_{\max} for NSL-fabricated Ag nanoparticles on glass ($D = 390$ nm; $d_m = 25$ nm) and mica substrates ($D = 390$ nm, $d_m = 35$ nm). (A) and (B) represent LSPR behavior of nanoparticles on glass substrate before N_2 flow and after a 24-h N_2 flow, respectively. The average measured LSPR λ_{\max} values are 703 ± 9.0 and 704 ± 7.0 nm, respectively. (C) and (D) represent LSPR behavior of nanoparticles on mica substrate before N_2 flow and after a 24-h N_2 flow, respectively. The average measured LSPR λ_{\max} values are 699 ± 5.0 and 698 ± 4.0 nm, respectively.

that the glass substrate, with its higher number density of surface oxide sites and more hydrophilic character, retains adsorbed water at relatively high surface coverage and, accordingly, has greater local dielectric inhomogeneity. Similarly, mica, with its lower number density of surface oxide sites and less hydrophilic character, retains adsorbed water at relatively low surface coverage with concomitantly greater local dielectric homogeneity.

Although it has been demonstrated that a large portion of the LSPR λ_{\max} variation is attributable to an adsorbed water layer, the experiments presented here inspire the hypothesis that at least three other factors may also be involved. First, without performing ultrahigh vacuum experiments, it is impossible to ensure that the adsorbed water layer is completely eliminated by 24 h of N_2 gas flow. Accordingly, adsorbed water may be responsible for a larger portion of the LSPR λ_{\max} distribution than demonstrated in Figure 4. Second, the natural or thiol-etch-induced LSPR λ_{\max} variation due to nanoparticle structural variations may also contribute to the residual variation. Third, the ramifications of weak electromagnetic coupling between nanoparticles are not fully understood and may also play a role in the LSPR λ_{\max} variation. Future experiments using ultrahigh vacuum conditions or near field scanning optical microscopy along with detailed electromagnetic simulations of the coupling effects will be undertaken to further clarify this issue.

SERS Enhancement Factor Calculation. The objective throughout this work is to produce the *most conservative possible* value of the EF consistent with the experimental data. The known spot size of the 20 \times microscope objective ($w = 4$ μm),²⁴ areal density for single-layer NSL-derived nanoparticles (7.2% coverage),¹ and nanoparticle size determine the number of nanoparticles in the observed area. The exposed surface area of each nanoparticle is calculated on the basis of its in-plane width a and out-of-plane height b (approximately the mass thickness d_m).

Assuming that each nanoparticle is a truncated tetrahedron, the exposed surface area is

$$A_{\text{surf}} = \sqrt{3}d_m(2a - d_m) + \frac{\sqrt{3}(a - d_m)^2}{3} \quad (1)$$

Next, taking the adsorbate benzenethiol as an example, the largest value of the packing density reported in the literature (6.8×10^{14} molecules/ cm^2)^{25,26} is used to calculate the maximum number of adsorbate molecules per nanoparticle. Any disorder in the self-assembled monolayer would lower the packing density, yielding a larger EF. The maximum number of molecules per nanoparticle and the total number of nanoparticles in the probe area determine the maximum surface number density (N_{surf}) of adsorbate molecules that contribute to the measured SER signal on each sample (viz., 2×10^6 benzenethiol molecules).

A neat, liquid sample of the adsorbate molecule in a thin glass cell was used as the Raman intensity standard. The probe volume of the confocal microscope with the 20 \times objective was found to be 7.5 pL (on the basis of $1/e^2$ analysis).²⁷ Using the density of the liquid sample, $\rho = 1.073$ g cm^{-3} for benzenethiol, the volume number density (N_{vol}) of molecules contributing to the normal Raman signal measured from the standard is 4×10^{13} benzenethiol molecules.

SERS EFs were calculated using the following equation:

$$\text{EF}(j, 1575 \text{ cm}^{-1}) = \left(\frac{N_{\text{vol}} I_{\text{surf}}}{N_{\text{surf}} I_{\text{vol}}} \right) \left(\frac{\text{LSPR amplitude}(j)}{\text{LSPR amplitude}(\text{average})} \right) \quad (2)$$

where I_{vol} and I_{surf} are the measured intensities, in analog/digital converter units per second per milliwatt, of the normal Raman standard and SER sample, respectively, and N_{surf} and N_{vol} are defined above. The first factor in eq 2 represents the traditional EF calculation.²⁸ A second factor must be included for studies on NSL-fabricated samples because they contain a small percentage of slip dislocations, point defects, and vacancies. Such defects reduce the number of nanoparticles contributing to the amplitude of the LSPR spectrum and, therefore, to the measured SERS signal. To account for the effects of defects, the EF is linearly corrected by the ratio of the measured amplitude for a particular extinction spectrum j to the average amplitude in that data set. The product of these two factors yields the surface EF that is plotted versus LSPR λ_{\max} . The resultant plot is the PS-SERE spectrum.

Excitation Wavelength Dependence. Figure 5 shows the correlated LSPR and SER spectra corresponding to the maxima of the PS-SERES experiments performed on NSL-fabricated samples with adsorbed benzenethiol using $\lambda_{\text{ex}} = 514.5$, 532.0, and 632.8 nm. These three examples show that the highest intensity SER spectra are achieved when the LSPR λ_{\max} is located between λ_{ex} and λ_{vib} . The EFs for the ν_{8a} (symmetric C–C ring stretch) mode²⁹ at 1575-cm^{-1} shift in spectra D, E, and F are 7.6×10^7 , 6.3×10^7 , and 9.0×10^7 , respectively.

Parts A–C of Figure 6 show PS-SERE spectra for the ν_{8a} mode of benzenethiol excited at $\lambda_{\text{ex}} = 514.5$, 532.0, and 632.8 nm, respectively. In each case, the paired extinction and SER spectra seen in Figure 5 generate the information necessary to define the optimized point for the PS-SERES plot. The PS-SERE spectra clearly show that the maximum SERS EFs occur when the LSPR λ_{\max} lies between λ_{ex} and λ_{vib} . However, the EF does not vary by more than a factor of 10 when the SERS signal is measurable above background. Attempts to capture SERS spectra from substrates with a LSPR λ_{\max} outside the x -axis LSPR ranges were unsuccessful. The solid line overlaid

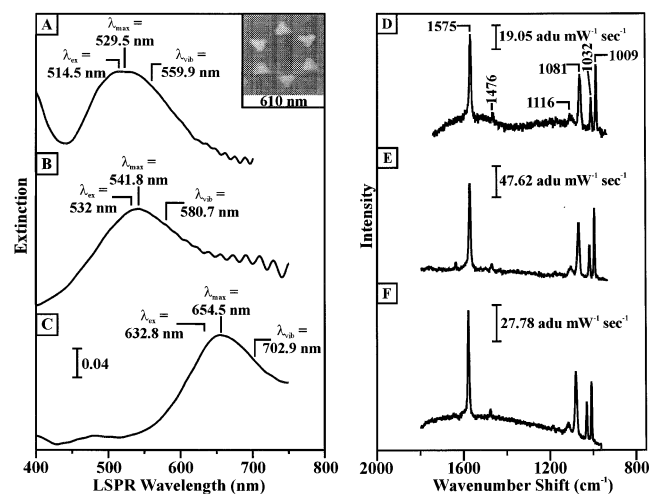


Figure 5. Correlated, spatially resolved LSPR and SER spectra of benzenethiol-dosed NSL substrates with maximized enhancement factors. (A) and (D) were measured from $D = 280$ nm, $d_m = 36$ nm Ag nanoparticles with 0.7 mW $\lambda_{\text{ex}} = 514.5$ nm. (B) and (E) were measured from $D = 280$ nm, $d_m = 36$ nm Ag nanoparticles with 0.7 mW $\lambda_{\text{ex}} = 532.0$ nm. (C) and (F) were measured from $D = 400$ nm, $d_m = 56$ nm Ag nanoparticles with 1.2 mW $\lambda_{\text{ex}} = 632.8$ nm. All LSPR spectra were captured with an integration time of 75 ms. Both the λ_{ex} and λ_{max} are denoted in each extinction spectrum. All Raman spectra were captured with an integration time of 30 s. Benzenethiol solutions were 1 mM, and dosing times were greater than 16 h.

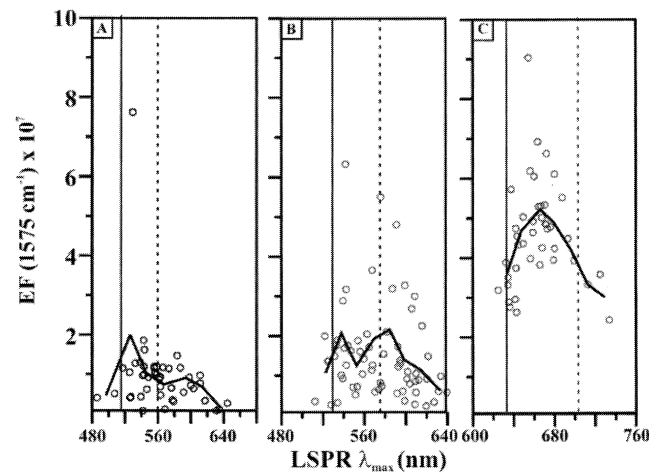


Figure 6. PS-SERES for the ν_{sa} (1575 cm^{-1}) band of benzenethiol with three different excitation wavelengths: (A) $\lambda_{\text{ex}} = 514.5$ nm, (B) $\lambda_{\text{ex}} = 532.0$ nm, and (C) $\lambda_{\text{ex}} = 632.8$ nm. For each λ_{ex} , both the wavelength location of the excitation (solid line) and the scattering (dashed line) are marked. The overlaid line represents the bin-averaged values of the LSPR λ_{max} and EF. Bin widths are (Figure 6A) 24 nm, (Figure 6B) 16 nm, and (Figure 6C) 16 nm.

on the PS-SERES data points represents the binned average values of the LSPR λ_{max} and EF. The bin widths were determined by dividing the LSPR λ_{max} data range by the square root of the number of data points. Note that, in all cases, there are a small number of data points representing EFs 2 – 4 times the average EF. To quantify the conditions for maximizing the EF within this window, we have calculated the LSPR λ_{max} range that yields the top 20% of the EF values. In plots in Figure 6A–C, these ranges are (Figure 6A) 529 – 583 nm (18904 – 17153 cm^{-1}), (Figure 6B) 539 – 615 nm (18553 – 16260 cm^{-1}), and (Figure 6C) 638 – 688 nm (15674 – 14535 cm^{-1}). All of the other vibrational modes of benzenethiol behave similarly.

It is important to note that the spectra depicted in this study are significantly different than those measured in single-

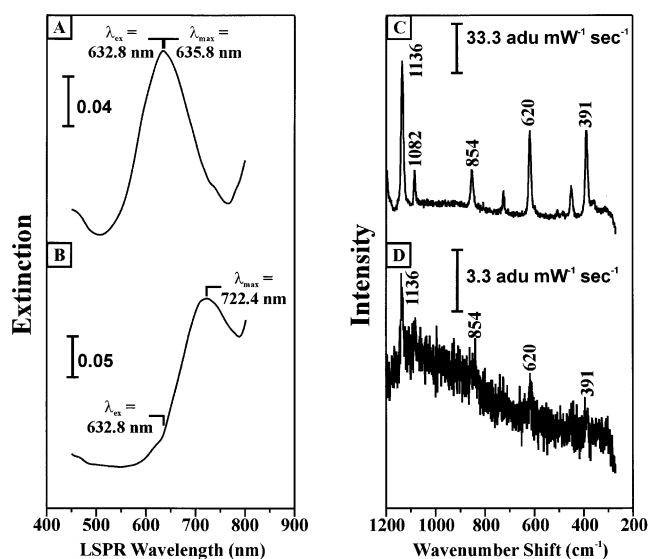


Figure 7. Correlated, spatially resolved LSPR and SER spectra of 3,4-dichlorobenzenethiol-dosed NSL substrates demonstrating SER spectra resulting from excitation both inside and outside the ~ 120 -nm window. (A) and (C) were measured from $D = 400$ nm, $d_m = 56$ nm Ag nanoparticles, and (B) and (D) were measured from $D = 400$ nm, $d_m = 20$ nm Ag nanoparticles. The 3,4-dichlorobenzenethiol solutions were 1 mM, and dosing times were greater than 16 h.

molecule SERS experiments. This is most evident when one considers that the measured SER spectrum does not vary over the 25 - μm -diameter spot size probed by the white light source during extinction measurements and that there are no evident temporal spectral fluctuations. This work investigates fundamental electromagnetic effects without being hindered by issues of site-to-site adsorbate motion and nonensemble averaged spectral characteristics. Figure 7 shows the SER spectra of 3,4-dichlorobenzenethiol resulting from laser excitation both inside and outside the high EF window. When λ_{ex} is close to the LSPR λ_{max} (Figure 7A,C), then the resulting EF is large (2×10^7), and when λ_{ex} is far from the LSPR λ_{max} (Figure 7B,D), then the resulting EF is comparatively small (1×10^6).

Molecular Adsorbate Dependence. To verify that these optimization conditions are molecularly general, PS-SERES investigations were performed using 3,4-dichlorobenzenethiol, 1,4-benzenedithiol, and $\text{Fe}(\text{bpy})_3^{2+}$ on Ag NSL-fabricated substrates. Each of these molecules is known to adsorb irreversibly to the Ag substrate. Figure 8 displays correlated extinction and SER spectra from the maximum of PS-SERES experiments for each of the aforementioned adsorbates. In all cases, high signal-to-noise ratio spectra are observed. The correlated extinction and SER spectra for 3,4-dichlorobenzenethiol are shown in Figure 8A,D. In this case, EFs were calculated using neat, liquid 3,4-dichlorobenzenethiol as the standard and the packing density of benzenethiol because no coverage measurements for 3,4-dichlorobenzenethiol have been reported in the literature. This assumption likely overestimates the packing density, and accordingly, underestimates the EF of 2.3×10^7 for the 1136 - cm^{-1} shift in-plane ring deformation mode of 3,4-benzenedithiol. The correlated extinction and SER spectra for 1,4-benzenedithiol are shown in Figure 8B,E. In this case, EFs were calculated using neat, liquid benzenethiol as the standard because 1,4-benzenedithiol is a solid and the packing density of benzenethiol since no coverage measurements for 1,4-benzenedithiol have been reported. Because benzenethiol

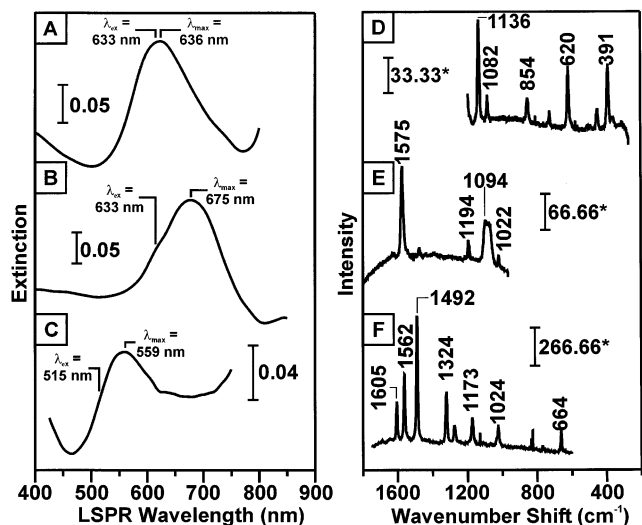


Figure 8. Correlated, spatially resolved LSPR and SER spectra of two other nonresonant adsorbates and one resonant adsorbate on NSL substrates with maximized enhancement factors. (A) and (D) show 3,4-dichlorobenzenethiol being adsorbed onto $D = 400$ nm, $d_m = 56$ nm Ag samples, $\lambda_{\text{ex}} = 632.8$ nm, and $P = 1$ mW. (B) and (E) show 1,4-benzenedithiol adsorbed onto $D = 400$ nm, $d_m = 52$ nm Ag samples, $\lambda_{\text{ex}} = 632.8$ nm, and $P = 1$ mW. (C) and (F) $\text{Fe}(\text{bpy})_3(\text{PF}_6)_2$ adsorbed onto $D = 310$ nm, $d_m = 52$ nm Ag samples, $\lambda_{\text{ex}} = 514.5$ nm, and $P = 0.5$ mW. All LSPR spectra were captured with an integration time of 75 ms. All Raman spectra were captured with an integration time of 30 s. The 3,4-dichlorobenzenethiol and 1,4-benzenedithiol solutions were 1 mM, while the $\text{Fe}(\text{bpy})_3(\text{PF}_6)_2$ solution was 0.4 mM. All dosing times were greater than 16 h. (*) represents units of $\text{adu mW}^{-1} \text{s}^{-1}$.

and 1,4-benzenedithiol are structurally similar, neither assumption is likely to significantly perturb the calculated EF of 1.4×10^8 for the 1094-cm^{-1} ν_2 symmetric C–C ring stretching mode of 1,4-benzenedithiol. The correlated extinction and surface-enhanced resonance Raman (SERR) spectra for $\text{Fe}(\text{bpy})_3^{2+}$ are shown in Figure 8C,F. In this case, EFs were calculated using the normal Raman spectrum of $\text{Fe}(\text{bpy})_3^{2+}$ solution excited outside the molecular resonance band with $\lambda_{\text{ex}} = 632.8$ nm. The experimentally measured packing density for $\text{Ru}(\text{bpy})_3^{2+}$ on Ag^{30} of 0.96×10^{14} molecules/ cm^2 was used to calculate the SERRS EF of 7.1×10^9 for the 1492-cm^{-1} shift ν_7 in-plane bipyridine ring vibration mode³¹ of $\text{Fe}(\text{bpy})_3^{2+}$.

It is clear from the data presented in Figure 8 that NSL-fabricated surfaces are effective SERS substrates for irreversibly bound adsorbates. Figure 9 shows a direct comparison between PS-SERE spectra for the same vibrational mode (the ν_2 symmetric C–C ring stretching mode)²⁹ in three related adsorbates: benzenethiol (Figure 9A), 1,4-benzenedithiol (Figure 9B), and 3,4-dichlorobenzenethiol (Figure 9C). In all cases, $\lambda_{\text{ex}} = 632.8$ nm. These spectra clearly show the same pattern seen in Figure 6 when λ_{ex} was varied. The EFs vary by less than a factor of 10 when the LSPR λ_{max} is within approximately a 120-nm window. As before, SERS spectra were not measurable above background from substrates with an LSPR λ_{max} outside the x -axis range shown. Overall, the optimized EFs are 1.0×10^8 , 1.3×10^8 , and 2.1×10^6 , respectively. Generally, the EF is relatively constant over the demonstrated LSPR λ_{max} window, yielding relatively lenient matching conditions. However, in each case, there are data points representing EF values that exceed the average by a factor of 2–3. To quantify the conditions for maximizing the EF within this window, we have calculated the LSPR λ_{max} range that yields the top 20% of the EF values. In plots in Figure 9A–C, these ranges are (Figure 9A) 649–680 nm ($15408\text{--}14706\text{ cm}^{-1}$), (Figure 9B) 635–730

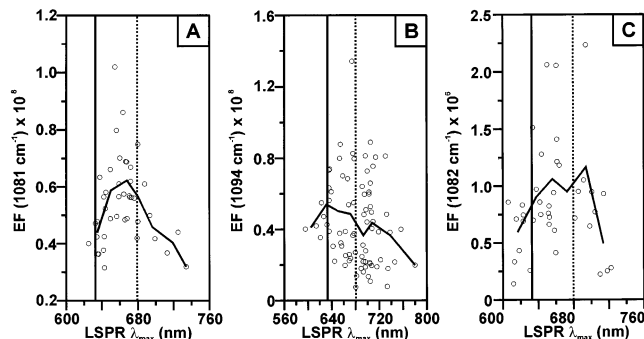


Figure 9. PS-SERES for the ν_2 mode of three different adsorbates on NSL substrates: (A) benzenethiol band at 1081 cm^{-1} , (B) 1,4-benzenedithiol band at 1094 cm^{-1} , and (C) 3,4-dichlorobenzenethiol band at 1082 cm^{-1} . In all cases, substrates were incubated in a 1-mM solution for greater than 12 h, $\lambda_{\text{ex}} = 632.8$ nm, and the integration time for each SER spectrum was 30 s. Incident powers were (A) 1.5 mW, (B) 1 mW, and (C) 1 mW. For each molecule, both the wavelength location of the excitation (solid line) and the scattering (dashed line) are marked. The overlaid line represents the bin-averaged values of the LSPR λ_{max} and EF. Bin widths are (A) 17 nm, (B) 21 nm, and (C) 19 nm.

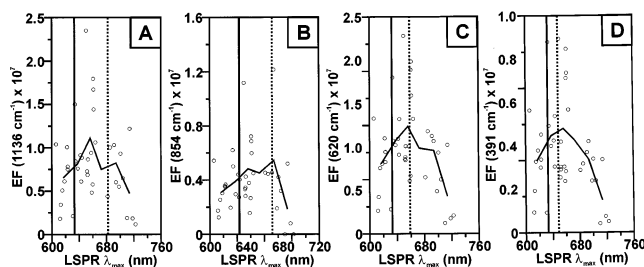


Figure 10. PS-SERES for four different vibrational bands of 3,4-dichlorobenzenethiol. (A) 1136 cm^{-1} , (B) 854 cm^{-1} , (C) 620 cm^{-1} , and (D) 391 cm^{-1} . In all cases, substrates were incubated in a 1-mM solution for greater than 12 h, $\lambda_{\text{ex}} = 632.8$ nm, incident power was 1 mW, and the integration time for each SER spectrum was 30 s. For each vibrational band, both the wavelength location of the excitation (solid line) and the scattering (dashed line) are marked. The overlaid line represents the bin-averaged values of the LSPR λ_{max} and EF. Bin widths are (A) 19 nm, (B) 19 nm, and (C) 19 nm.

nm ($15748\text{--}13699\text{ cm}^{-1}$), and (Figure 9C) 634–694 nm ($15773\text{--}14409\text{ cm}^{-1}$). The assumption that the benzenethiol packing density can be applied to the 3,4-dichlorobenzenethiol experiment is likely the source of the significantly lower EFs shown in Figure 8C because the chlorine substituents decrease the molecular packing density. Though it is impossible to know without a coverage measurement for 3,4-dichlorobenzenethiol on Ag, this variance in EF could also be a signature of the SERS chemical enhancement mechanism.³²

Vibrational Mode Dependence. To verify that various vibrational modes adhere to the demonstrated behavior, PS-SERE spectra were measured for five different vibrational modes of 3,4-dichlorobenzenethiol. Note that the data for all five bands are derived from the same set of NSL samples and SER spectra. PS-SERES plots for four of the five bands are displayed in Figure 10, while the fifth is shown in Figure 9C. The five bands, in descending cm^{-1} shift order, correspond to the following molecular motions: in-plane ring deformation (Figure 10A), ring breathing mode (Figure 9C), another ring deformation (Figure 10B), the C–S stretch (Figure 10C), and the C–Cl stretch (Figure 10D). All five PS-SERE spectra demonstrate optimized EFs with the same LSPR λ_{max} . In all five cases, the maximized EF is 2–3 times larger than the average EF (overlaid line in Figures 10A–D). Again, samples with LSPR λ_{max} values

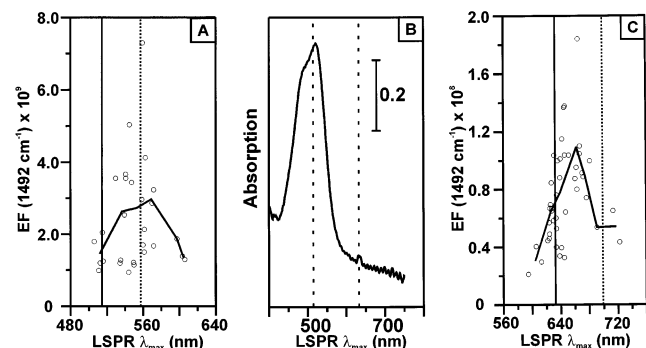


Figure 11. PS-SERES for both SERR and SER spectra of $\text{Fe}(\text{bpy})_3\text{-(PF}_6)_2$ adsorbed onto NSL substrates. (A) The excitation profile when λ_{ex} (514.5 nm) meets the molecular resonance condition (SERRS). (B) The absorption spectrum of 0.4-mM $\text{Fe}(\text{bpy})_3\text{-(PF}_6)_2$ solution in methanol (C) The excitation profile when λ_{ex} (632.8 nm) does not meet the molecular resonance condition (SERS). In both cases, substrates were incubated in a 0.4-mM solution for 10 min. In the SERR spectra collected for (A), incident power was 0.5 mW and integration times were 1 s. In the SER spectra collected for (B), incident power was 1 mW and integration times were 30 s. The absorption spectrum for $\text{Fe}(\text{bpy})_3\text{-(PF}_6)_2$ is inset with both excitation wavelengths marked. For both excitation profiles, both the wavelength location of the excitation (solid line) and the scattering (dashed line) are marked. The overlaid line represents the bin-averaged values of the LSPR λ_{max} and EF. Bin widths are (A) 19 nm and (C) 19 nm.

less than 600 nm or greater than 760 nm yielded no measurable SERS signal above background. To quantify the conditions for maximizing the EF within this window, we have calculated the LSPR λ_{max} range that yields the top 20% of the EF values. In plots in Figure 10A–D, these ranges are (Figure 10A) 634–714 nm (15773–14006 cm^{-1}), (Figure 10B) 606–694 nm (16502–14409 cm^{-1}), (Figure 10C) 606–664 nm (16502–15060 cm^{-1}), and (Figure 10D) 606–664 nm (16502–15060 cm^{-1}).

Resonant vs Preresonant PS-SERES. The recent use of resonance Raman adsorbates in single-molecule SERS studies⁷ has rekindled interest in understanding the relationship between the adsorbate-localized molecular resonance and the nanoparticle-localized LSPR. To improve our understanding of this relationship, PS-SERES experiments were carried using $\text{Fe}(\text{bpy})_3^{2+}$ as the adsorbate. $\text{Fe}(\text{bpy})_3^{2+}$ is an efficient resonant Raman scatterer with a metal-to-ligand charge-transfer absorption band centered at 520 nm (see Figure 11B). Resonant PS-SERES measurements were made using $\lambda_{\text{ex}} = 514.5$ nm (Figure 11A), and a second set of preresonant PS-SERES measurements were made using $\lambda_{\text{ex}} = 632.8$ nm (Figure 11C). Both PS-SERE spectra demonstrate the same energy matching conditions seen under all other circumstances as well as some EFs two to four times larger than the average EF values (overlaid line). To quantify the conditions for maximizing the EF within this window, we have calculated the LSPR λ_{max} range that yields the top 20% of the EF values. In plots in Figure 11A,C, these ranges are (Figure 11A) 529–562 nm (18904–17794 cm^{-1}) and (Figure 11C) 642–667 nm (15576–14993 cm^{-1}). Overall, the maximized SERRS EF is approximately 40 times larger than the maximized SERS EF. To determine the nature of the molecule-localized and nanoparticle-localized enhancement mechanisms, a resonant Raman spectrum (RRS) and a preresonant Raman spectrum (Pre-RRS) were also measured for $\text{Fe}(\text{bpy})_3^{2+}$. In this case, the $\text{Fe}(\text{bpy})_3^{2+}$ solution was placed in a thin cell under the confocal microscope; no SERS substrate was present. When comparing $\text{EF}_{\text{RRS}}/\text{EF}_{\text{Pre-RRS}}$ for $\text{Fe}(\text{bpy})_3^{2+}$ solutions, approximately the same EF ratio, 40, is measured. This is interpreted as evidence that the molecule-localized

electronic resonance does not damp the nanoparticle-localized LSPR. Further work is needed to establish the generality of this result and to examine the important case where the adsorbate electronic resonance has molecule-to-nanoparticle charge-transfer character.

Conclusions

The systematic study presented here accomplishes two goals. First, we demonstrate that nanosphere lithography (NSL) derived Ag nanoparticles are effective surface-enhanced Raman-scattering (SERS) substrates. Plasmon sampled surface-enhanced Raman excitation spectra (PS-SERES) plots for varied molecular adsorbates demonstrate that high signal-to-noise SER spectra can be obtained from NSL-fabricated substrates when the narrow localized surface plasmon resonance (LSPR) is properly correlated with the chosen excitation wavelength. In fact, these spectra display the largest SERS EFs measured to date on nanostructured substrates, $\text{EF} \geq 1 \times 10^8$. Second, it is clearly demonstrated that it is necessary to correlate nanoparticle structural data and LSPR spectroscopic information in order to effectively implement SERS on nanostructured surfaces with narrow LSPR line widths. Using nanoparticle substrates that are structurally well characterized, the relationship between the LSPR λ_{max} and the SERS EF is correlated in both resonant and nonresonant PS-SERES. The PS-SERES behavior was studied as a function of: (1) excitation wavelength (514.5, 532.0, and 632.8 nm), (2) molecular adsorbate (benzenethiol, 1,4-benzenedithiol, 3,4-dichlorobenzenethiol, and $\text{Fe}(\text{bpy})_3^{2+}$), (3) vibrational band (aromatic ring, C–S stretch, and C–Cl stretch modes), and (4) molecular resonance or nonresonance excitation. The PS-SERE spectra reveal that the largest SERS EF is achieved when the energy corresponding to the narrow LSPR λ_{max} falls within ~ 120 -nm window that includes the energy of the excitation wavelength and the scattered photons.

In this work, naturally occurring nanoparticle structural and local dielectric variations caused by adsorbed water layers on glass substrates are exploited. The dielectric inhomogeneities result in a distribution of LSPR λ_{max} values having a standard deviation of ~ 10 nm. Comparison of the LSPR λ_{max} distribution for Ag nanoparticles deposited on two different substrates, glass and mica, demonstrate that significantly smaller standard deviation occurs on mica as compared to glass substrates. Since mica is less hydrophilic than glass, this observation supports the assertion of the influence of an adsorbed water layer.

Measured PS-SERE spectra for a series of adsorbates, including 3,4-dichlorobenzenethiol, 1,4-benzenedithiol, and $\text{Fe}(\text{bpy})_3^{2+}$ allow us to conclude that this ~ 120 -nm LSPR λ_{max} window is not limited to just one type of adsorbate. Further work is required to establish full molecular generality. In each case, high signal-to-noise SER spectra with large EFs were achieved. Direct comparison of a single vibrational mode in three related molecules (benzenethiol, 1,4-benzenedithiol, and 3,4-dichlorobenzenethiol) with the same excitation wavelength shows that the PS-SERE spectra follow the same pattern in each case. Only in one case was an optimized EF $\sim 10^2$ times lower than was observed in all other cases. This is likely the consequence of coverage and/or orientation factors. Comparison of the PS-SERE spectra for different vibrational modes within a given adsorbate molecule demonstrates that modes differing greatly in energy (391- cm^{-1} shift versus 1136- cm^{-1} shift) share the same LSPR λ_{max} condition necessary to achieve optimized EFs.

The adsorbate $\text{Fe}(\text{bpy})_3^{2+}$ is used to directly compare the resonant and preresonant PS-SERES cases. SERRS is probed

with 514.5-nm excitation, and preresonant SERS is probed with 632.8-nm excitation. The resonant and preresonant PS-SERES follow similar patterns of behavior. Also the optimized SERRS EF is ~ 40 times larger than the optimized SERS EF. This observation illustrates that this adsorbate, with its molecule-localized electronic transition, does not damp the LSPR and that the SERS and RRS effects appear to act multiplicatively.

In each of the cases presented, the PS-SERES follow a pattern where correlation of the substrate LSPR λ_{max} allows achievement of high S/N ratio SER spectra. It is important to note that in all PS-SERE spectra collected to date, including those presented herein, a small percentage of measured EFs fall significantly above (viz., 1–4 times) the average EF values. While this occurrence is repeatable from sample to sample and for different excitation wavelengths, adsorbates, vibrational modes, and electronic resonance conditions, its cause is currently unknown and under active investigation.

Acknowledgment. The authors acknowledge support from the National Science Foundation (EEC-0118025 and DMR-0076097), the Air Force Office of Scientific Research MURI program (F49620-02-1-0381), an ACS Division of Analytical Chemistry fellowship sponsored by GlaxoSmithKline (C.L.H.), and a Northwestern University Presidential Fellowship (C.L.H.). We thank Prof. G. C. Schatz and A. D. McFarland for many helpful conversations and technical assistance.

References and Notes

- (1) Haynes, C. L.; Van Duyne, R. P. *J. Phys. Chem. B* **2001**, *105*, 5599–5611.
- (2) Duval Malinsky, M.; Kelly, L.; Schatz, G. C.; Van Duyne, R. P. *J. Am. Chem. Soc.* **2001**, *123*, 1471–1482.
- (3) Haes, A. J.; Van Duyne, R. P. *J. Am. Chem. Soc.* **2002**, *124*, 10596–10604.
- (4) Jensen, T. R.; Duval Malinsky, M.; Haynes, C. L.; Van Duyne, R. P. *J. Phys. Chem. B* **2000**, *104*, 10549–10556.
- (5) Schatz, G. C.; Van Duyne, R. P. In *Handbook of Vibrational Spectroscopy*; Griffiths, P. R., Ed.; Wiley: New York, 2002; Vol. 1, pp 759–774.
- (6) Campion, A.; Kambhampati, P. *Chem. Soc. Rev.* **1998**, *27*, 241–250.
- (7) Nie, S.; Emory, S. R. *Science* **1997**, *275*, 1102–1106.
- (8) Kneipp, K.; Wang, Y.; Kneipp, H.; Perelman, L. T.; Itzkan, I.; Dasari, R. R.; Feld, M. S. *Phys. Rev. Lett.* **1997**, *78*, 1667–1670.
- (9) Jeanmaire, D. L.; Van Duyne, R. P. *J. Electroanal. Chem.* **1977**, *84*, 1–20.
- (10) Liao, P. F.; Bergman, J. G.; Chemla, D. S.; Wokaun, A.; Melngailis, J.; Hawryluk, A. M.; Economou, N. P. *Chem. Phys. Lett.* **1981**, *81*, 355–359.
- (11) Gregory, B. W.; Clark, B. K.; Standard, J. M.; Avila, A. *J. Phys. Chem. B* **2001**, *105*, 4684–4689.
- (12) Otto, A.; Mrozek, I.; Grabhorn, H.; Akemann, W. *J. Phys. Condens. Matter* **1992**, *4*, 1143–1212.
- (13) Liao, P. F.; Stern, M. B. *Opt. Lett.* **1982**, *7*, 483–485.
- (14) Weitz, D. A.; Garoff, S.; Gramila, T. J. *Opt. Lett.* **1982**, *7*, 168–170.
- (15) Hulteen, J. C.; Treichel, D. A.; Smith, M. T.; Duval, M. L.; Jensen, T. R.; Van Duyne, R. P. *J. Phys. Chem. B* **1999**, *103*, 3854–3863.
- (16) Piner, R. D.; Zhu, J.; Xu, F.; Hong, S.; Mirkin, C. A. *Science* **1999**, *283*, 661–663.
- (17) Salmeron, M.; Hendrick, B. *Surf. Rev. Lett.* **1999**, *6*, 1275–1281.
- (18) Miranda, P. B.; Xu, L.; Shen, Y. R.; Salmeron, M. *Phys. Rev. Lett.* **1998**, *81*, 5876–5879.
- (19) Jensen, T. R.; Schatz, G. C.; Van Duyne, R. P. *J. Phys. Chem. B* **1999**, *103*, 2394–2401.
- (20) Jensen, T. R.; Duval, M. L.; Kelly, L.; Lazarides, A.; Schatz, G. C.; Van Duyne, R. P. *J. Phys. Chem. B* **1999**, *103*, 9846–9853.
- (21) Noguera, C. *Physics and Chemistry at Oxide Surfaces*; Cambridge University Press: Cambridge, 1996.
- (22) Fussa-Rydell, O.; Zhang, H.-T.; Hupp, J. T.; Leidner, C. R. *Inorg. Chem.* **1988**, *28*, 1533–1537.
- (23) Hulteen, J. C. I. *Surface-Enhanced Hyper-Raman Spectroscopy 2. Nanosphere Lithography*. Ph.D. Thesis, Northwestern University, Evanston, Illinois, 1995.
- (24) Jensen, T. R. *Optical Characterization of Nanofabricated Silver Films: Surface Plasmon Resonance and Surface-Enhanced Spectroscopy*. Ph.D. Thesis, Northwestern University, Evanston, Illinois, 1999.
- (25) Wan, L.-J.; Terashima, M.; Noda, H.; Osawa, M. *J. Phys. Chem. B* **2000**, *104*, 3563–3569.
- (26) Whelan, C. M.; Smyth, M. R.; Barnes, C. J. *Langmuir* **1999**, *15*, 116–126.
- (27) Nie, S.; Zare, R. N. *Ann. Rev. Biophys. Biomol. Struct.* **1997**, *26*, 567–596.
- (28) Van Duyne, R. P. In *Chemical and Biochemical Applications of Lasers*; Moore, C. B., Ed.; Academic Press: New York, 1979; Vol. 4, pp 101–184.
- (29) Varsanyi, G. *Vibrational Spectra of Benzene Derivatives*; Academic Press: New York, 1969.
- (30) Stacy, A. M.; Van Duyne, R. P. *Chem. Phys. Lett.* **1983**, *102*, 365–370.
- (31) Maruszewski, K.; Bajdor, K.; Strommen, D. P.; Kincaid, J. R. *J. Phys. Chem.* **1995**, *99*, 6286–6293.
- (32) Kambhampati, P.; Child, C. M.; Foster, M. C.; Campion, A. J. *Chem. Phys.* **1998**, *108*, 5013–5026.